Macromolecules

pubs.acs.org/Macromolecules Article

Tuning Porosity in Triptycene-Poly(arylene ether)s

Kayla R. Storme, Benedikt S. Schreib, Zachary P. Smith,* and Timothy M. Swager*

Cite This: *Macromolecules* 2024, 57, 7065−7073 Read Online

ACCESS | Metrics & More | Article Recommendations | Supporting Information

ABSTRACT: We report a scalable synthesis of high-molecular-weight poly(arylene ether)s (PAEs) using decafluorobiphenyl under S_NAr reaction conditions and the preparation of enantiopure (*R*,*R*)-6,11-di(*tert*-butyl)triptycene-1,4-hydroquinone. The nonfluorinated biphenyl-based PAE was also synthesized using Pd-catalyzed C−O coupling methods, and structure−property comparisons were made from the different biphenyl-based polymers. The integration of free-volume-promoting triptycene moieties on the main chain gives rise to intrinsic porosity, which can be further modulated by incorporating biphenyl or perfluorobiphenyl comonomers. The nonfluorinated PAE exhibited a BET surface area of 270 $m^2\ g^{-1}$, whereas the racemic and enantiopure fluorinated PAEs showed higher BET surface areas of 454 and 368 $m^2\ g^{-1}$, respectively. WAXS analysis revealed that all of the polymers tested have a greater disruption of chain packing compared to related polyimides, with the fluorinated PAEs having the highest average interchain spacing. The fluorinated PAEs also demonstrated high gas permeability as a result of their free volume. The triptycene-based PAEs also were resistant to plasticization even at CO_2 pressures of ∼31 bar.

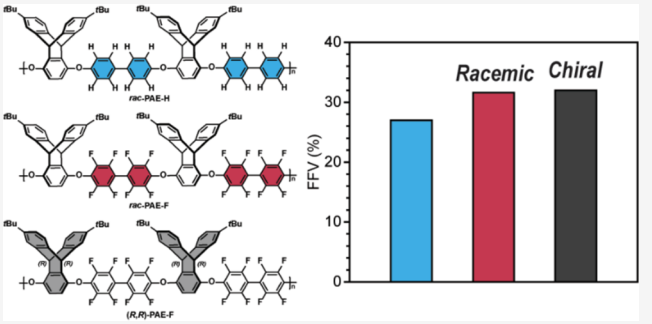

INTRODUCTION

Triptycenes and related [2.2.2] and [2.2.1] bicyclic systems are configurationally rigid 3D structures that can promote a high internal free volume in polymers when they are incorporated directly within or fused to the main chain. These design principles have been leveraged to make intrinsically microporous polymers with targeted materials properties, including materials with low dielectric constants,[1−3] high fluorescence quantum yields for efficient excitonic transport,[4] superior ion transport,[5,6] attractive properties for highly active heterogeneous catalyst supports,[7,8] and enhanced gas transport.[9,10] In terms of gas separations, when triptycene is introduced into a polyimide backbone, the fractional free volume and rigidity simultaneously increase,[2] resulting in enhanced gas permeability and reduced plasticization effects.[11,12] Similar improvements have been demonstrated for other polymers, as well. For example, a triptycene-based polysulfone had improved permeability, selectivity, and resistance to physical aging compared to bisphenol A-based polysulfone.[13] Moreover, benzotriptycene-based polymers of intrinsic microporosity (PIMs) recently redefined the CO_2/CH_4 and CO_2/N_2 upper bounds.[10]

Similar to polyimides, poly(arylene ether)s (PAEs) are promising materials for gas separations because of their excellent thermal, mechanical, and chemical stability.[14,15] Traditional PAE syntheses use S_NAr reactions that employ activated aryl fluoride monomers.[1,16] Long et al. demonstrated that triptycene units disrupt chain packing in PAEs, thereby increasing the free volume of the polymer. In that study, one of the subject PAEs was first synthesized by the S_NAr reaction of decafluorobiphenyl and 6,11-di(*tert*-butyl)triptycene-1,4-hydroquinone to make *rac*-PAE-F.[1] The high free volume in this system resulted in lower dielectric constants compared to a commercial, highly cross-linked polyphenylene known as SiLK.[1,17] However, gas separations with *rac*-PAE-F have yet to be investigated. In 2002, Shibasaki and Ueda developed a Pd-catalyzed polycondensation method to synthesize PAEs from a bisphenol and nonactivated 4,4′-dibromobiphenyl.[18] Guo et al. recently optimized this Pd-catalyzed C−O polycondensation method to also accommodate hydroquinones as substrates to diversify accessible PAE structures.[19] This polycondensation methodology enabled us to synthesize *rac*-PAE-H (Scheme 1b), the hydrocarbon analogue to *rac*-PAE-F, thereby providing two structural analogues of polymers with systematic differences between biphenyl composition: one sample fluorinated and the other sample hydrocarbon-based.

Previous studies on polyimides and polysulfones showed that polymers featuring *meta* structural connectivity demonstrate higher permselectivities in gas transport compared to their *para* isomers, indicating a relationship between isomeric effects and gas transport.[20−24] Additionally, Aitken et al.

Received: May 27, 2024
Revised: July 12, 2024
Accepted: July 22, 2024
Published: August 1, 2024

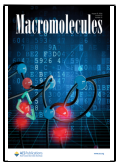

https://doi.org/10.1021/acs.macromol.4c01199
Macromolecules 2024, 57, 7065−7073

Scheme 1. Polymerization Reaction Schemes for (a) *rac*-PAE-F, (b) *rac*-PAE-H, and (c) (*R*,*R*)-PAE-F; (d) Structures of the 6FDA-Based Polymers Referenced for Comparisons[25−28]

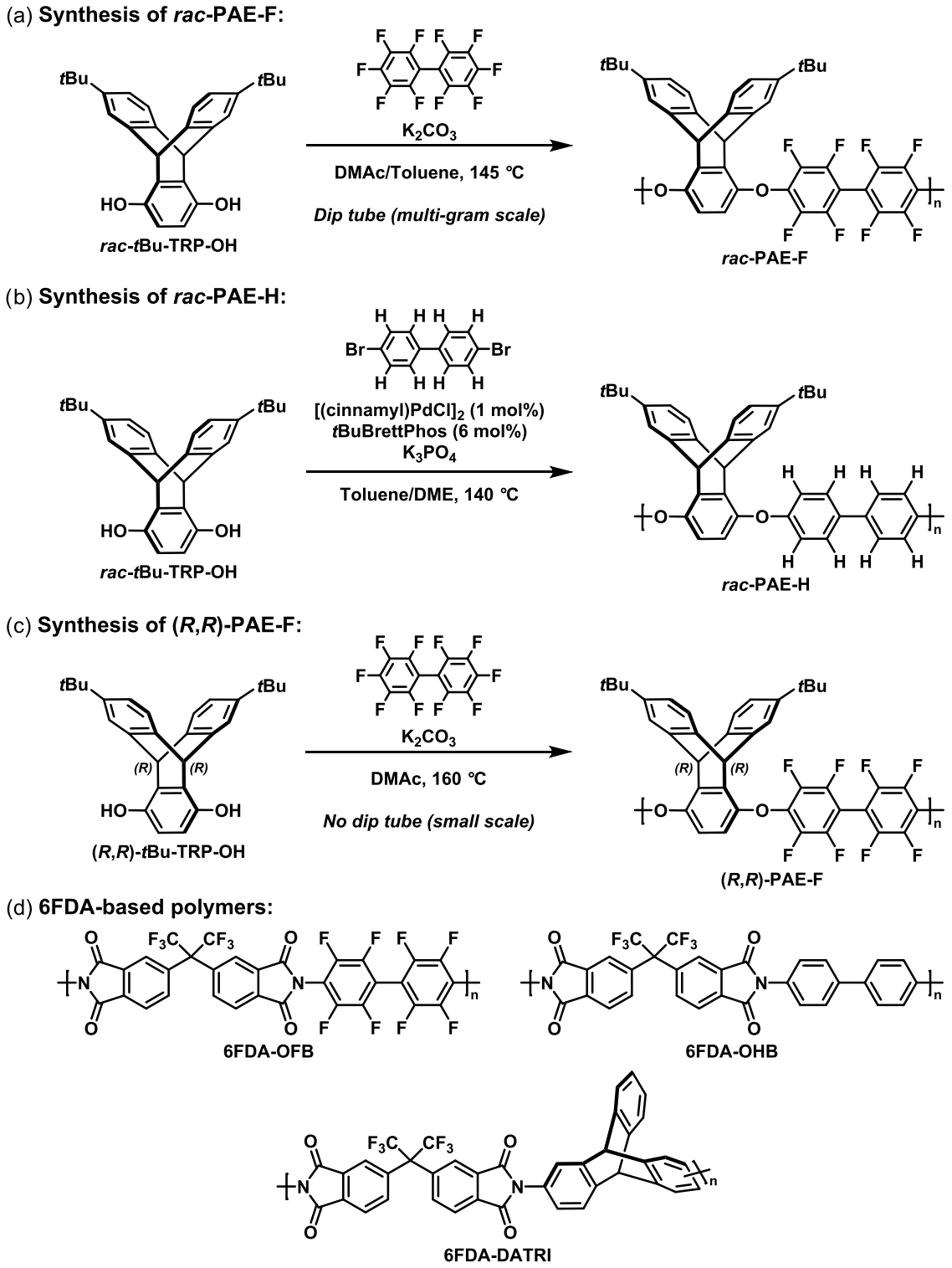

observed that incorporating unsymmetric features into the polymer chain lowered the glass transition temperatures and promoted efficient chain packing.[20] To the best of our knowledge, the differences in porosity for racemic and enantiopure polymer structures have not yet been considered, so we also synthesized the (*R*,*R*)-6,11-di(*tert*-butyl)triptycene-1,4-hydroquinone enantiomer ((*R*,*R*)-*t*Bu-TRP-OH) and polymerized it with decafluorobiphenyl to produce the enantiopure polymer (*R*,*R*)-PAE-F (Scheme 1c). An enantiopure polymer may exhibit more uniform polymer chain packing compared to the corresponding racemic polymer, thereby impacting the porosity and separation performance. For comparison, Scheme 1d shows the structures of three 6FDA-based polyimides reported in the literature[25−28] that have similar structural groups to those of the PAEs. This study

https://doi.org/10.1021/acs.macromol.4c01199
Macromolecules 2024, 57, 7065−7073

compares these related polyimides to the PAEs synthesized in this work.

In this study, we report the optimized S_NAr synthesis of *rac*-PAE-F at larger (multigram) scale to produce molecular weights considerably higher than those previously reported,[1] the synthesis of the analogous *rac*-PAE-H that contains C−H functionality instead of C−F functionality, and the synthesis of an enantiopure monomer, (*R*,*R*)-*t*Bu-TRP-OH, and its corresponding chiral polymer, (*R*,*R*)-PAE-F. Structure−property relationships of these PAE analogues were investigated through comparisons of thermal properties, BET surface area, and fractional free volume. It was found that *rac*-PAE-H was an intrinsically microporous polymer because the free volume-generating triptycene units inhibit the dense packing of the biphenyl moieties. Perfluorobiphenyl groups boost the BET surface area and promote greater free volume in *rac*-PAE-F and (*R*,*R*)-PAE-F. Films of *rac*-PAE-H, *rac*-PAE-F, and (*R*,*R*)-PAE-F were fabricated, but *rac*-PAE-H resulted in brittle films that ruptured at ∼1 bar of pressure. As a result, we report pure-gas performance for *rac*- and (*R*,*R*)-PAE-F and compare our results to those of related structures reported in the literature.

EXPERIMENTAL SECTION

Materials. All materials were used as received unless otherwise noted. Potassium phosphate was purchased from Alfa Aesar. Decafluorobiphenyl was purchased from Alfa Aesar and recrystallized in hexanes before use. Palladium(π-cinnamyl) chloride dimer, *N*,*N*-dimethylacetamide (DMAc, 99.8%), ethyl acetate (≥99.5%), chloroform, dichloromethane, pyridine, and inhibitor-free anhydrous 1,2-dimethoxyethane (99.5%) were purchased from Sigma-Aldrich. *t*BuBrettPhos and (1*S*)-(−)-camphanic chloride were purchased from Ambeed. Hexanes and methanol were purchased from Macron Fine Chemicals. Ethanol was purchased from VWR. Anhydrous toluene (99.85%) was purchased from Fisher Scientific. Hydrochloric acid (37%) solution in water was purchased from Sigma-Aldrich and diluted with deionized water to make a 3 M solution. 4,4′-Dibromobiphenyl was purchased from Sigma-Aldrich and recrystallized from petroleum ether. 6,11-Di(*tert*-butyl)triptycene-1,4-hydroquinone (*rac*-*t*Bu-TRP-OH) was purchased from Akita Innovations and purified via recrystallization with ethyl acetate and hexanes. All gases used for testing (He, H_2, CH_4, N_2, O_2, and CO_2) were of ultrahigh purity from Airgas.

Synthetic Procedures. *Synthesis of rac-PAE-F.* A 100 mL resin kettle fitted with a dip tube, thermocouple, and short-path distillation apparatus was charged with *rac*-*t*Bu-TRP−OH (7.157 g, 18.0 mmol, 1.0 equiv) and decafluorobiphenyl (6.000 g, 18.0 mmol, 1.0 equiv). Then, DMAc (60 mL) and toluene (7.5 mL) were poured into the resin kettle, followed by K_2CO_3 (5.708 g, 41.3 mmol, 2.3 equiv). The dip tube was adjusted to a position below the solvent level so argon would sparge the solution. The receiving flask fixed to the distillation apparatus was placed into a dry ice/acetone bath. The solution was stirred with argon bubbling through the dip tube to distill off the water−toluene azeotrope and concentrate the polymerization solution. The resin kettle was heated to 145 °C for 2.5 h. Once cooled to room temperature, the viscous solution was precipitated into boiling HCl water (pH ∼ 2 to 3) to neutralize the remaining carbonate and promote polymer aggregation. The polymer fibers were collected and dried using vacuum filtration before redissolving in THF. The THF solution was precipitated into DI water and polymer fibers were recovered via vacuum filtration. Residual DMAc remained in the fibers, so the fibers were dissolved in chloroform, precipitated into methanol, and collected via vacuum filtration. The fibers were dried in a vacuum oven at 200 °C for 48 h before characterizing (yield: 10.87 g, 83.6%). ^{1}H NMR (500 MHz, $CDCl_3$) δ 7.50, 7.49, 7.39, 7.37, 7.08, 7.08, 7.07, 7.07, 6.49, 6.48, 5.99, 1.26; ^{13}C NMR (126 MHz, $CDCl_3$) δ 148.81, 148.43, 145.93, 144.47, 143.87, 142.81, 141.67, 140.91, 138.31, 136.69, 123.64, 122.25, 121.64, 113.81, 47.83, 34.77, 31.62, 1.17; ^{19}F NMR (471 MHz, $CDCl_3$) δ −137.86, −137.88, −137.91, −137.93, −152.94, −152.95, −152.99, −153.01.

Synthesis of rac-PAE-H. Synthesis of PAE-H followed previously reported procedures.[5] For the synthesis, *rac*-*t*Bu-TRP-OH (200.0 mg, 0.502 mmol, 1.0 equiv) and 4,4′-dibromobiphenyl (156.6 mg, 0.502 mmol, 1.0 equiv) were used to yield 115 mg (39.6%) of pink powder. ^{1}H NMR (500 MHz, $CDCl_3$) δ 7.54, 7.53, 7.52, 7.52, 7.27, 7.24, 7.22, 7.02, 7.02, 7.00, 7.00, 6.98, 6.98, 6.98, 6.97, 6.96, 6.74, 6.72, 6.71, 5.66, 5.65, 5.64, 1.24, 1.23; ^{13}C NMR (126 MHz, $CDCl_3$) δ 158.12, 148.39, 147.14, 147.11, 147.07, 147.04, 144.75, 142.01, 140.18, 140.15, 135.05, 134.95, 128.94, 128.53, 128.22, 128.16, 126.97, 123.58, 121.87, 121.62, 118.91, 118.84, 117.53, 117.46, 48.22, 34.75, 31.68.

Synthesis of (R,R)-tBu-TRP-OR.* A round-bottom flask under ambient atmosphere was charged with *rac*-*t*Bu-TRP-OH (3.99 g, 10.0 mmol, 1.00 equiv), and pyridine was added in portions until a clear solution was obtained (ca. 70 mL total, the reaction was stirred for 10 min between additions due to the slow rate of dissolution). (1*S*)-(−)-Camphanic chloride (5.42 g, 25.0 mmol, 2.50 equiv) was added in one portion, and the reaction was stirred for 48 h at 20 °C. Chloroform (250 mL) was added to the reaction mixture, and the organic phase was washed with water (2 × 300 mL), 1 M aq HCl (2 × 300 mL), and brine (1 × 300 mL). The organic phase was dried over Na_2SO_4 and concentrated under reduced pressure. Toluene (100 mL) was added to the residue and removed under reduced pressure to remove residual pyridine.

The crude material was dissolved in boiling dichloromethane (ca. 500 mL). Next, the solution was concentrated to about one-third of the volume on a rotary evaporator at 40 °C, cooled to 4 °C, and the resulting precipitate was collected by filtration and washed with a small amount of cold dichloromethane. This procedure was repeated one additional time to afford (*R*,*R*)-*t*Bu-TRP-OR* as a white solid (3.37 g containing 15 wt % dichloromethane, 3.77 mmol, 38% yield, >20:1 dr by ^{1}H NMR analysis). ^{1}H NMR (500 MHz, CD_2Cl_2) δ 7.38, 7.38, 7.28, 7.27, 7.09, 7.08, 7.07, 7.07, 6.87, 5.42, 2.74, 2.73, 2.72, 2.71, 2.71, 2.71, 2.69, 2.68, 2.40, 2.39, 2.38, 2.37, 2.37, 2.36, 2.35, 2.14, 2.13, 2.12, 2.11, 2.11, 2.10, 2.09, 2.08, 1.88, 1.87, 1.86, 1.85, 1.84, 1.83, 1.82, 1.27, 1.27, 1.26, 1.24, 1.22; ^{13}C NMR (126 MHz, CD_2Cl_2) δ 178.07, 166.37, 149.46, 144.05, 143.01, 141.32, 139.93, 123.92, 122.80, 121.76, 119.88, 91.33, 55.34, 55.05, 48.93, 34.90, 31.55, 29.43, 17.37, 17.27, 9.95.; MS (JEOL AccuTOF 4G LC-plus equipped with an ionSense DART source): *m*/*z* calculated for $C_{48}H_{54}O_8$ $[M]^+$ 758.3813, found 758.3913; O. R. $[\alpha]_D^{20}$ = +16.0 (*c* 0.33, THF).

Single crystals suitable for X-ray diffraction were obtained by vapor diffusion (dichloromethane/hexanes).

Synthesis of (R,R)-tBu-TRP-OH. A Schlenk flask was charged with ethanol (80 mL) and sparged with argon for 20 min while stirring rapidly. To the flask were added the diastereopure triptycene derivative (*R*,*R*)-*t*Bu-TRP-OR* obtained in the previous step (3.27 g, 3.65 mmol, 1.00 equiv) and potassium carbonate (1.00 g, 7.24 mmol, 1.83 equiv). The reaction was stirred at room temperature for 16 h, quenched by the addition of water (ca. 200 mL) and ethyl acetate (ca. 300 mL), and acidified by the addition of ca. 10 mL of 1 M aq HCl (pH of the aqueous phase was about 7, checked using pH paper). The organic layer was separated, washed with brine (1 × 150 mL), dried over Na_2SO_4, and concentrated to afford a brown oil. Chloroform (50 mL) was added, the resulting suspension was sonicated for 10 min, and the precipitate was collected by filtration, washed with additional chloroform, and dried under vacuum. In order to remove residual chloroform, the product was dissolved in a small amount of ethyl acetate, the solution was concentrated under reduced pressure, and the resulting solid was dried under vacuum at 120 °C for 12 h to afford (*R*,*R*)-*t*Bu-TRP-OH as an off-white/faint red powder (1.06 g containing ca. 5 wt % ethyl acetate, 2.53 mmol, 69%). ^{1}H NMR (500 MHz, DMSO-d_6) δ 8.77, 7.40, 7.40, 7.29, 7.27, 6.97, 6.97, 6.96, 6.95, 6.30, 5.73, 1.21.; ^{13}C NMR (126 MHz, DMSO-d6) δ 147.22, 145.76, 144.70, 143.01, 132.29, 122.98, 120.97, 120.49, 112.78, 46.49, 34.21, 31.31; O. R. $[\alpha]_D^{20}$ = +18.7 (*c* 1.0, THF). The enantiomeric excess was confirmed to be >99% by HPLC analysis

https://doi.org/10.1021/acs.macromol.4c01199
Macromolecules 2024, 57, 7065−7073

Scheme 2. (a) Synthesis of (*R*,*R*)-*t*Bu-TRP-OH and (b) Side- and Bottom-View ORTEP Diagrams of (*R*,*R*)-*t*Bu-TRP-OR*[a]

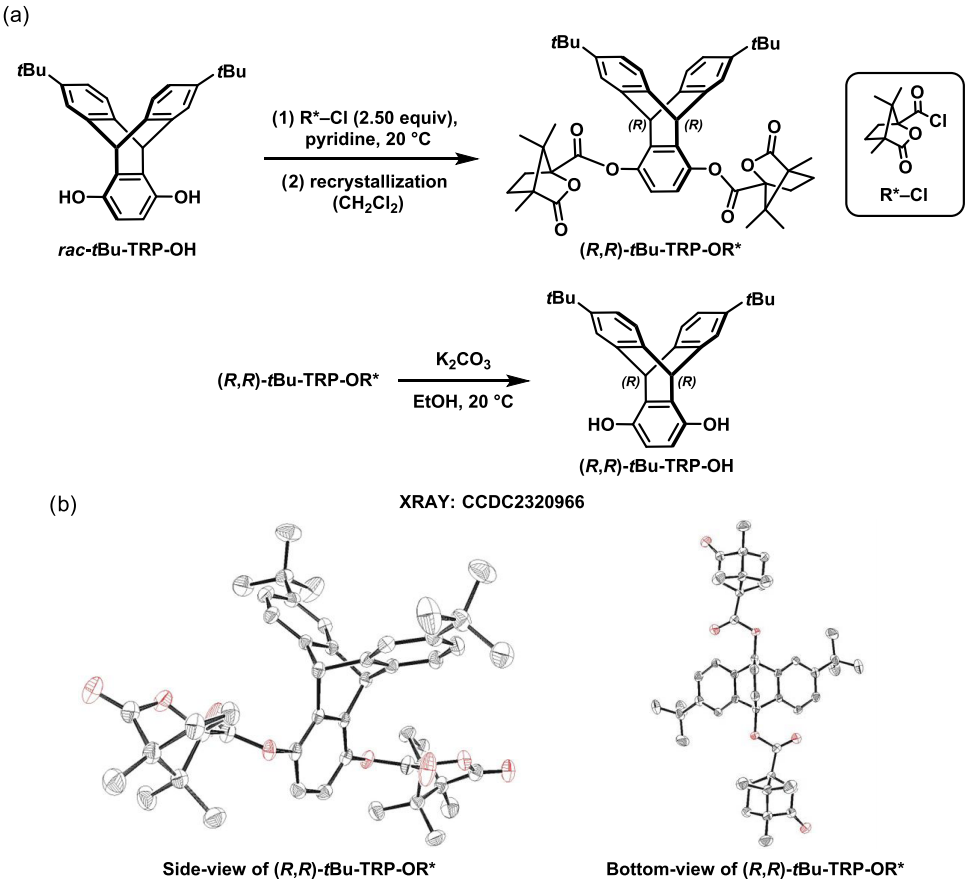

[a]Atomic displacement parameters at 100 K are drawn at 70% probability level. Hydrogen atoms and dichloromethane molecules are omitted for clarity.

(Chiralpak IA column, 25% isopropanol in hexanes, 1 mL per minute, detection at 250 nm).

Synthesis of (R,R)-PAE-F. A flame-dried 100 mL round-bottom flask was equipped with a reflux condenser and charged with a magnetic stir bar, (*R*,*R*)-*t*Bu-TRP-OH (containing ca. 5 wt % ethyl acetate, 1.369 g, 3.26 mmol, 1.00 equiv), and decafluorobiphenyl (1.090 g, 3.26 mmol, 1.00 equiv). The flask was evacuated and backfilled with argon gas three times, and then anhydrous *N*,*N*-dimethylacetamide (30 mL) was added. The reaction was stirred at room temperature until all reagents dissolved. Potassium carbonate (1.036 g, 7.50 mmol, 2.30 equiv) was added and the reaction was heated to 160 °C while stirring. After 3 h, the reaction was allowed to cool to ca. 80 °C and precipitated by dropwise addition to an aqueous 1 M HCl solution (300 mL). The precipitate was collected by vacuum filtration, washed with aqueous 1 M HCl, dried, redissolved in tetrahydrofuran (ca. 30 mL), and precipitated from deionized water (300 mL). The resulting precipitate was collected by vacuum filtration, washed with deionized water, and dried under vacuum at 140 °C for 4 h to afford the polymer as white fibers (yield: 2.18 g, 92.5%). ^{1}H NMR (500 MHz, $CDCl_3$) δ 7.50, 7.38, 7.08, 6.51−6.43, 5.99, 1.33−1.23; ^{13}C NMR (126 MHz, $CDCl_3$) δ 148.81, 148.44, 145.93, 144.48, 143.87, 142.90, 141.67, 140.90, 138.31, 136.69, 123.64, 122.25, 121.64, 113.82, 102.69, 47.84, 34.77, 31.62, 30.47; ^{19}F NMR (471 MHz, $CDCl_3$) δ −137.86, −137.88, −137.90, −137.92, −152.93, −152.95, −152.98, −153.00. O. R. $[\alpha]_D^{20}$ = −32.0 (*c* 1.0, THF).

RESULTS AND DISCUSSION

The syntheses of *rac*-PAE-F and *rac*-PAE-H using S_NAr and Pd-catalyzed C−O coupling conditions, respectively, are shown in Scheme 1a,b. Toluene was added to the S_NAr reaction mixture to form an azeotrope with water produced during the polymerization, which was removed from the reaction mixture via distillation. Effective removal of the water is important to prevent potential hydroxide reactions with the perfluorobiphenyl monomer and to maintain a 1:1 monomer equivalence to maximize molecular weight. Our scale-up of the polymerization makes use of a stainless-steel dip tube that was inserted with its outlet below the solvent line to bubble argon *in situ* through the reaction mixture. For the reaction, 19.5 w/v % of monomer and a short-path distillation apparatus were used to collect the distillate (Figure S1). During the polymerization, toluene and water are distilled from the reaction and into the receiving flask, resulting in an increase in the concentration of the reaction solution to approximately 26% over the course of the polymerization. Under these conditions, we obtained M_n = 74.2 kDa for *rac*-PAE-F (Scheme 1a). When employing the dip tube method on small scales, rapid concentration of the reaction occurs, leading to solvent loss that hinders proper reagent mixing and results in a low-molecular-weight polymer (M_n = 6.76 kDa). Other attempts starting with more concentrated solutions and/or without use of the dip tube yielded polymer at or below ∼32 kDa for M_n, which is consistent with the previously reported polymerization.[1] Thus, these improved reaction conditions enable us to access high molecular weights that are required for membrane film formation, which will be discussed later.

https://doi.org/10.1021/acs.macromol.4c01199
Macromolecules 2024, 57, 7065−7073

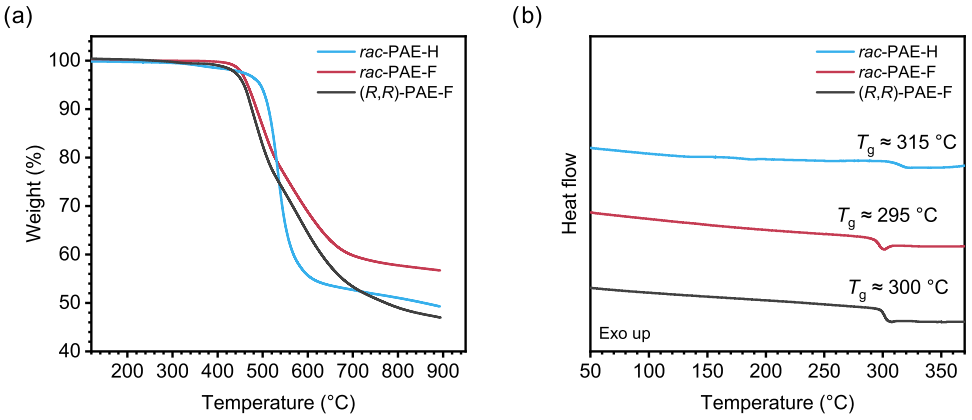

Figure 1. Heating curves for (a) TGA and (b) last heating cycle of DSC for *rac*-PAE-H, *rac*-PAE-F, and (*R*,*R*)-PAE-F.

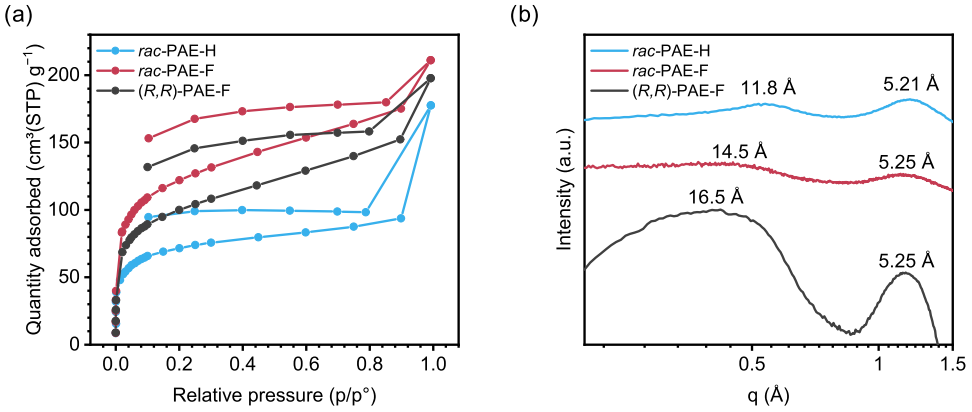

Figure 2. (a) N_2 adsorption isotherms at 77 K for *rac*-PAE-H, *rac*-PAE-F, and (*R*,*R*)-PAE-F. (b) WAXS spectra results for *rac*-PAE-H, *rac*-PAE-F, and (*R*,*R*)-PAE-F.

4,4′-Dibromobiphenyl is an unactivated aryl bromide and unsuitable for S_NAr reactions, so we followed the previously reported Pd-catalyzed polycondensation[19] to polymerize *rac*-*t*Bu-TRP-OH and 4,4′-dibromobiphenyl and yielded M_n = 15.6 kDa *rac*-PAE-H (Scheme 1b). Scheme 2a shows the chiral separation of (*R*,*R*)-*t*Bu-TRP-OH, which is inspired by the separation of chiral iodotriptycenes.[29] First, (1*S*)-(−)-camphanic chloride (R*-Cl) was installed through an esterification reaction with *rac*-*t*Bu-TRP-OH to produce a mixture of *t*Bu-TRP-OR* diastereomers. The *t*Bu-TRP-OR* diastereomers were readily separated via recrystallization in dichloromethane, eliminating the need for chromatographic purification. The chiral auxiliary was then removed through ethanolysis to yield the (*R*,*R*)-*t*Bu-TRP-OH enantiomer. The enantiomer's absolute configuration was determined via single-crystal X-ray analysis of the intermediate (Scheme 2b). Since we synthesized a limited amount of (*R*,*R*)-*t*Bu-TRP-OH, we performed the S_NAr polymerization with (*R*,*R*)-*t*Bu-TRP-OH at a small scale following the previously reported procedure[1] without a dip tube to afford M_n = 16.0 kDa of (*R*,*R*)-PAE-F (Scheme 1c). Unlike *rac*-PAE-H, films of (*R*,*R*)-PAE-F were stable up to 51 bar.

Thermal Properties of PAEs. The synthesized polymers displayed high thermal stability characteristics of PAEs with degradation temperatures (T_d) above 450 °C (Figure 1a). The glass transition temperature (T_g) is higher in *rac*-PAE-H than in *rac*-PAE-F or (*R*,*R*)-PAE-F (Figure 1b). This feature may be indicative of the tighter packing of polymer chains for *rac*-PAE-H relative to both PAE-F polymers, and potentially from secondary interactions such as $\pi-\pi$ stacking.[30,31] The preferred solid-state conformation for biphenyl has been reported to be approximately coplanar,[25,30,32,33] and this coplanar conformation is stabilized by the delocalization of π-electrons[34] and/or by an attractive H−H bonding interaction between the 2,2′-Hs of the biphenyl.[35] A coplanar conformation can promote $\pi-\pi$ stacking arrangements[31] in *rac*-PAE-H. In contrast, the 2,2′-F atoms in perfluorobiphenyl experience steric repulsion, which causes perfluorobiphenyl to adopt a conformation with an ∼45° dihedral angle between the phenyl groups.[25] The similar T_d's and T_g's of *rac*-PAE-F and (*R*,*R*)-PAE-F suggest both PAE-F polymers likely have a similar morphology.

Free Volume and Packing Structure Analysis. To evaluate the packing structure of *rac*-PAE-H, *rac*-PAE-F, and (*R*,*R*)-PAE-F, we measured the BET surface areas and calculated the fractional free volume (FFV). BET is often used as an indirect but highly correlated indicator of the microporosity of a PIM material, and surface areas typically scale with increasing free volume. FFV describes the "empty space" resulting from inefficient chain packing. All of the PAEs have characteristic Type I isotherms (Figure 2a) with increasing pressure, indicating that these materials are high free volume polymers. There is also pronounced hysteresis upon depressurization, suggesting a potential dilation effect at high N_2 activities or potentially some mesoporous characteristic in the packed polymer powder. The measured surface area of *rac*-PAE-F was 454 $m^2\ g^{-1}$, (*R*,*R*)-PAE-F was 368 $m^2\ g^{-1}$, and *rac*-PAE-H was 270 $m^2\ g^{-1}$ (Table S1), indicating that the PAE-F polymers have more porosity to accommodate small

https://doi.org/10.1021/acs.macromol.4c01199
Macromolecules 2024, 57, 7065−7073

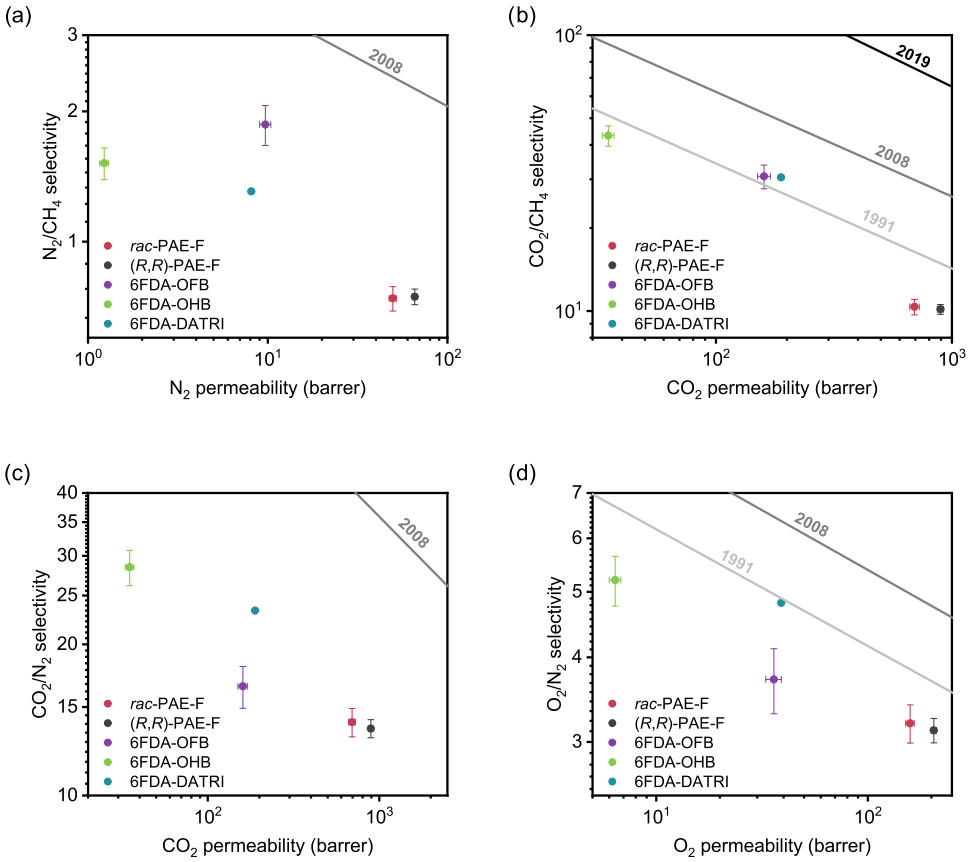

Figure 3. Robeson upper bounds for pure-gas permeation of *rac*-PAE-F and (*R*,*R*)-PAE-F compared to 6FDA-OHB,[25] 6FDA-OFB,[25] and 6FDA-DATRI[28] for (a) N_2/CH_4, (b) CO_2/CH_4, (c) CO_2/N_2, and (d) O_2/N_2.

molecules relative to *rac*-PAE-H. A similar interpretation was found by calculating FFV through group contribution methods,[36] with the PAE-F polymers having a higher FFV than that of *rac*-PAE-H (Table S1). We anticipate that these findings relate to the nonplanar conformation of perfluorobiphenyl inhibiting chain packing. Wu et al. investigated the difference in morphology and transport for polyimides that contained either fluorinated or hydrocarbon-based biphenyl residues and reported a 50% increase in FFV for a polyimide with a fluorinated biphenyl group (6FDA-OFB) compared to the nonfluorinated analogue (6FDA-OHB).[25] The greater free volume was attributed to the nonplanar conformation of perfluorobiphenyl. Zhang et al. also noted an increase in FFV and *d*-spacing in a copolyimide containing 2,2′-bis-(trifluoromethyl) biphenyl compared to one containing unsubstituted biphenyl.[37] We note that the FFV of *rac*-PAE-H, *rac*-PAE-F, and (*R*,*R*)-PAE-F is higher than that of 6FDA-OFB, 6FDA-OHB,[25] and 6FDA-DATRI,[28] affirming that *t*Bu-triptycene as a residue enhances free volume in addition to the enhanced FFV effects from fluorine.

To investigate the physical packing structure of the polymers, we collected WAXS spectra for each sample. The polymers were amorphous, and the films were optically clear. In WAXS, diffuse scattering from voids between polymer chains is responsible for the peaks at lower q values, whereas scattering from intersegmental spacing produces peaks at higher q values (Figure 2b).[38] The peak centered at 14.5 Å in *rac*-PAE-F shifts to 11.8 Å in *rac*-PAE-H in accordance with the BET and free volume trends noted previously. (*R*,*R*)-PAE-F exhibits more defined peaks than the racemic PAEs and the largest *d*-spacing at 16.5 Å, indicating that (*R*,*R*)-PAE-F has a weaker packing structure compared to *rac*-PAE-F. All of these amorphous halos are centered at *d*-spacing values that are larger than those observed for the related 6FDA-based polymers (Scheme 1d).[25,28] Again, this finding indicates the free-volume-generating feature of *t*Bu-triptycene residues. We attributed the secondary signal at 5.21 Å for *rac*-PAE-H and 5.25 Å for the PAE-F polymers to interchain correlations as these distances are longer than would be expected for cofacial $\pi-\pi$ stacking.[39] This finding is also consistent with the triptycene moieties inhibiting close packing of the polymer chains and with triptycene moieties providing access to configurational free volume for molecular transport.[39−41]

Pure-Gas Permeation Analysis. Increases in permeability correlate with higher FFV, and as expected, the PAE-F polymers demonstrate higher permeability than 6FDA-OFB, 6FDA-OHB,[25] and 6FDA-DATRI[28] (Figure 3). Notably, (*R*,*R*)-PAE-F exhibited higher permeability than *rac*-PAE-F despite having an FFV within error of *rac*-PAE-F. Correspondingly, selectivity was inversely correlated with FFV. We observed a decrease in N_2/CH_4, CO_2/CH_4, CO_2/N_2, and O_2/N_2 selectivity for both PAE-F polymers relative to the 6FDA-based polymers. This finding suggests an increase in diffusivity for all gases within the higher-free-volume PAE materials; therefore, we calculated the diffusion coefficients using the time-lag method (Table S3). Interestingly, a small difference between the diffusivities was observed for (*R*,*R*)-PAE-F and *rac*-PAE-F and both have greater than 8-fold increase in CH_4 diffusion compared to 6FDA-OFB and 6FDA-DATRI. According to free volume theory, the logarithm of

https://doi.org/10.1021/acs.macromol.4c01199
Macromolecules 2024, 57, 7065−7073

diffusivity, log D, is a linear function of 1/FFV.[42−45] Figure S2 contains semilog diffusivity plots that show the increasing magnitude of the slopes ((0.255) O_2 < (0.304) CO_2 < (0.334) N_2 < (0.414) CH_4) correspond to the effective permeability diameter of the gas (O_2 (3.44 Å) < CO_2 (3.63 Å) < N_2 (3.66 Å) < CH_4 (3.81 Å)). Furthermore,diffusion correlations for (*R*,*R*)-PAE-F and *rac*-PAE-F are similar to those observed for the isomeric effects between *meta* and *para* connectivity in polysulfones and polyimides.[20−24]

The (*R*,*R*)-PAE-F polymer had higher diffusivities for all gases considered compared to the *rac*-PAE-F sample. These trends correlated with the small difference in FFV, but they were in contrast to the lower BET surface area values for (*R*,*R*)-PAE-F. This finding suggests that transport is dominated by diffusion, but that there is also a subtle trade-off in sorption and diffusion for enantiopure and racemic polymers that contributes to the overall permeabilities and permselectivities for these samples. Sorption of all gases is higher in 6FDA-OFB compared to 6FDA-DATRI, indicating that octafluorobiphenyl residues provide a greater boost in sorption than triptycene. CH_4 sorption back-calculated from time-lag analysis is 52% higher in *rac*-PAE-F than in 6FDA-OFB, but both polymers exhibit the same CO_2 sorption. (*R*,*R*)-PAE-F shows 44% higher CH_4 sorption and 21% lower CO_2 sorption. Figure S3 depicts the gas sorption plotted against the critical temperature, T_c, of each gas at 1 atm for the PAEs and 6FDA-based polymers considered in this study. A smaller slope is typically observed for perfluorinated polymers compared to hydrocarbon-based polymers, which have an expected baseline slope of ∼0.019 K^{-1} at infinite dilution.[42,46,47] We observed slopes that were lower than that observed for hydrocarbon-based polymers but were similar between each polymer considered in this study (Figure S3). This finding indicates that there is no correlation between sorption or T_c with fluorine content in these materials, likely because these materials are highly glassy.

Fluorinated polymers typically exhibit N_2/CH_4 selectivity higher than 1;[42,48,49] however, both PAE-F polymers demonstrate a selectivity less than 1 for N_2/CH_4. From the framework of the dual-mode sorption model,[50] this finding indicates that the higher CH_4/N_2 sorption selectivity is likely attributed to the nonequilibrium sorption mode, which overwhelms contributions from N_2/CH_4 diffusivity selectivity. The N_2/CH_4 diffusivity selectivity is approximately 2-fold lower in *rac*-PAE-F compared to 6FDA-OFB and 6FDA-DATRI, indicating that the greater free volume in *rac*-PAE-F reduces its size-sieving capabilities and thus results in a switch in permselectivity for the N_2/CH_4 pair. A similar difference in CO_2/CH_4 diffusivity selectivity is observed in (*R*,*R*)-PAE-F compared to 6FDA-OFB and 6FDA-DATRI. The CO_2/CH_4 sorption selectivity of *rac*-PAE-F and (*R*,*R*)-PAE-F polymers is similar to that of 6FDA-DATRI and 34 to 44% lower than 6FDA-OFB, respectively, suggesting decafluorobiphenyl and 6FDA moieties increase selectivity for CO_2 more than triptycene. Additionally, *rac*-PAE-F exhibits a CO_2/N_2 sorption selectivity that is 23% higher than that of 6FDA-DATRI and 24% lower than that of 6FDA-OFB. The CO_2/N_2 sorption selectivity of (*R*,*R*)-PAE-F was 28% higher than that of 6FDA-OFB and 2 factors higher than that of 6FDA-DATRI, respectively. Although diffusion was a clear correlating variable with transport properties (Figure S2), we did not observe a correlation between the sorption selectivity and volume fraction of fluorine (Figure S4).

The enhanced sorption selectivity may arise from interactions of CO_2 with the free volume generated by the 6FDA moieties, which are known to produce some of the highest CO_2-sorptive polyimides.[51] In fact, 6FDA-based polyimides are easily plasticized by CO_2 due to strong gas−polymer affinity.[27,52] This phenomenon results in a pure-gas CO_2 plasticization pressure of 8 bar for 6FDA-DATRI.[27] Subjecting *rac*-PAE-F to high-pressure sweeps of CO_2 reveals a plasticization pressure point of ∼31 bar (Figure 4), a nearly 4-

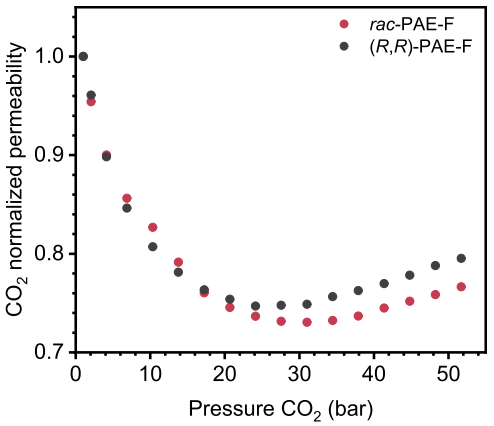

Figure 4. Pure-gas CO_2 permeabilities for the high-pressure sweep of *rac*-PAE-F and (*R*,*R*)-PAE-F.

fold improvement from that of 6FDA-DATRI, demonstrating that pairing perfluorobiphenyl with triptycene motifs can enhance resistance to CO_2-induced plasticization. The plasticization pressure point of (*R*,*R*)-PAE-F was observed at ∼24 bar. Although subtle, the slight difference in these plasticization pressure points correlates with the higher BET surface area and higher CO_2 sorption coefficient (cf., Figure 2a and Table S3) for *rac*-PAE-F. It is well known that plasticization pressure points occur when increases in diffusion overcome decreases in sorption for glassy polymers.[53−55] The slightly higher sorption of CO_2 in *rac*-PAE-F likely obscures the rise in diffusion for this polymer until higher pressures. In addition to the normalized plasticization pressure response in Figure 4, Figure S5 includes the full-scale CO_2 permeability versus pressure response. Solid-state dynamics characterization will elevate our understanding of changes in packing structure that occur in the presence of CO_2 in addition to mixed-gas permeation and sorption experiments, which will be the focus of future studies of the PAE-F motif.

CONCLUSIONS

We report a synthetic method in this study to improve the molecular weight of a previously reported PAE[1] in addition to the synthesis of the nonfluorinated analogue using recently developed Pd-catalyzed polycondensation. We also detail a method that yields enantiopure triptycene-based monomers used to produce (*R*,*R*)-PAE-F. Furthermore, we performed a comparative characterization study between the fluorinated and nonfluorinated PAEs formed through the same synthetic mechanism to assess structure−property relationships. Triptycene moieties dependably enhanced the free volume and microporosity, as demonstrated by FFV and BET analysis. Our WAXS results also indicated that perfluorobiphenyl structures further disrupt chain packing compared to nonfluorinated biphenyl analogues. Both PAEs have higher FFVs compared to

https://doi.org/10.1021/acs.macromol.4c01199
Macromolecules 2024, 57, 7065−7073

polyimide counterparts, resulting in increased permeability for *rac*-PAE-F and (*R*,*R*)-PAE-F. No plasticization pressure effects were observed up to ∼24 bar for (*R*,*R*)-PAE-F and ∼31 bar for *rac*-PAE-F, demonstrating resistance to plasticization for this class of materials.

■ ASSOCIATED CONTENT

Supporting Information

The Supporting Information is available free of charge at https://pubs.acs.org/doi/10.1021/acs.macromol.4c01199.

^{1}H, ^{13}C, ^{19}F NMR, optical rotation, circular dichroism, crystallographic data, X-ray diffraction data, CO_2 pressure sweep plots, tabulated SEC, TGA, DSC, BET, FFV, and density data, tabulated permeation data, and diffusion and sorption coefficients calculated using the time-lag method and sorption−diffusion model (PDF)

Accession Codes

CCDC 2320966 contains the supplementary crystallographic data for this paper. This data can be obtained free of charge via www.ccdc.cam.ac.uk/data_request/cif, by emailing data_request@ccdc.cam.ac.uk, or by contacting The Cambridge Crystallographic Data Centre, 12 Union Road, Cambridge CB2 1EZ, U.K.; fax: + 44 1223 336033.

■ AUTHOR INFORMATION

Corresponding Authors

Zachary P. Smith − *Department of Chemical Engineering, Massachusetts Institute of Technology, Cambridge, Massachusetts 02139, United States;* orcid.org/0000-0002-9630-5890; Email: zpsmith@mit.edu

Timothy M. Swager − *Department of Chemistry, Massachusetts Institute of Technology, Cambridge, Massachusetts 02139, United States;* orcid.org/0000-0002-3577-0510; Email: tswager@mit.edu

Authors

Kayla R. Storme − *Department of Chemistry, Massachusetts Institute of Technology, Cambridge, Massachusetts 02139, United States;* orcid.org/0000-0003-4520-9281

Benedikt S. Schreib − *Department of Chemistry, Massachusetts Institute of Technology, Cambridge, Massachusetts 02139, United States;* orcid.org/0000-0001-8201-0330

Complete contact information is available at: https://pubs.acs.org/10.1021/acs.macromol.4c01199

Notes

The authors declare no competing financial interest.

■ ACKNOWLEDGMENTS

The synthetic design of materials to incorporate pore architecture was supported by the National Science Foundation DMR-2207299, the NSF I-Corps program 2324992, and the U.S. Department of Energy, Office of Science, Office of Basic Energy Sciences, Separation Science program through award number DE-SC0019087. The authors also gratefully acknowledge the Office of Naval Research under award number N00014-21-1-2666 for developing strategies related to site-specific CO_2 binding. This material is based upon work supported by the National Science Foundation under Award No. 2146422. K.R.S. acknowledges support from the National Science Foundation Graduate Research Fellowship under grant number 1745302. B.S.S. acknowledges support from the Swiss National Science Foundation (Postdoc.Mobility P500PN_210768). Dr. Peter Mueller (MIT) is gratefully acknowledged for acquiring, solving, and refining crystallographic data.

■ REFERENCES

(1) Long, T. M.; Swager, T. M. Molecular Design of Free Volume as a Route to Low-κ Dielectric Materials. *J. Am. Chem. Soc.* **2003**, *125* (46), 14113−14119.

(2) Sydlik, S. A.; Chen, Z.; Swager, T. M. Triptycene Polyimides: Soluble Polymers with High Thermal Stability and Low Refractive Indices. *Macromolecules* **2011**, *44* (4), 976−980.

(3) Hsiao, S.-H.; Wang, H.-M.; Chen, W.-J.; Lee, T.-M.; Leu, C.-M. Synthesis and Properties of Novel Triptycene-Based Polyimides. *J. Polym. Sci. A Polym. Chem.* **2011**, *49* (14), 3109−3120.

(4) Yang, J.-S.; Swager, T. M. Porous Shape Persistent Fluorescent Polymer Films: An Approach to TNT Sensory Materials. *J. Am. Chem. Soc.* **1998**, *120* (21), 5321−5322.

(5) Moh, L. C. H.; Goods, J. B.; Kim, Y.; Swager, T. M. Free Volume Enhanced Proton Exchange Membranes from Sulfonated Triptycene Poly(ether ketone). *J. Membr. Sci.* **2018**, *549*, 236−243.

(6) Kim, Y.; Moh, L. C. H.; Swager, T. M. Anion Exchange Membranes: Enhancement by Addition of Unfunctionalized Triptycene Poly(ether sulfone)s. *ACS Appl. Mater. Interfaces* **2017**, *9*, 42409−42414.

(7) Guo, S.; Wu, Y.; Luo, S. X. L.; Swager, T. M. Versatile Nanoporous Organic Polymer Catalyst for the Size-Selective Suzuki-Miyaura Coupling Reaction. *ACS Appl. Nano Mater.* **2022**, *5* (12), 18603−18611.

(8) Liu, R. Y.; Guo, S.; Luo, S. X. L.; Swager, T. M. Solution-Processable Microporous Polymer Platform for Heterogenization of Diverse Photoredox Catalysts. *Nat. Commun.* **2022**, *13* (1), No. 2775.

(9) Weidman, J. R.; Luo, S.; Breier, J. M.; Buckley, P.; Gao, P.; Guo, R. Triptycene-Based Copolyimides with Tailored Backbone Rigidity for Enhanced Gas Transport. *Polymer* **2017**, *126*, 314−323.

(10) Comesaña-Gándara, B.; Chen, J.; Bezzu, C. G.; Carta, M.; Rose, I.; Ferrari, M. C.; Esposito, E.; Fuoco, A.; Jansen, J. C.; McKeown, N. B. Redefining the Robeson Upper Bounds for CO_2/CH_4 and CO_2/N_2 Separations Using a Series of Ultrapermeable Benzotriptycene-Based Polymers of Intrinsic Microporosity. *Energy Environ. Sci.* **2019**, *12* (9), 2733−2740.

(11) Li, F.; Zhang, C.; Weng, Y. Preparation and Gas Separation Properties of Triptycene-Based Microporous Polyimide. *Macromol. Chem. Phys.* **2019**, *220* (10), 1−7.

(12) Cho, Y. J.; Park, H. B. Gas Separation Properties of Triptycene-Based Polyimide Membranes. In *Modern Applications in Membrane Science and Technology*; American Chemical Society, 2011; pp 107−128.

(13) Corrado, T.; Huang, Z.; Aboki, J.; Guo, R. Microporous Polysulfones with Enhanced Separation Performance via Integration of the Triptycene Moiety. *Ind. Eng. Chem. Res.* **2020**, *59* (12), 5351−5361.

(14) Yee, A. F.; Smith, S. A. Molecular Structure Effects on the Dynamic Mechanical Spectra of Polycarbonates. *Macromolecules* **1981**, *14* (1), 54−64.

(15) Boyer, R. F. *Molecular Basis of Transitions and Relaxations*; CRC Press, 1978.

(16) Labadie, J. W.; Hedrick, J. L. New Activating Groups for Poly(aryl ether) Synthesis. *Makromol. Chemie. Macromol. Symp.* **1992**, *54-55* (1), 313−330.

(17) Martin, S. J.; Godschalx, J. P.; Mills, M. E.; Shaffer, E. O., II; Townsend, P. H. Development of a Low-Dielectric-Constant Polymer for the Fabrication of Integrated Circuit Interconnect. *Adv. Mater.* **2000**, *12* (23), 1769−1778.

(18) Shibasaki, Y.; Ueda, M. Synthesis of Poly(Aryl Ether) by Pd-Catalyzed Polycondensation. *Chem. Lett.* **2002**, *31* (8), 794−795.

(19) Guo, S.; Swager, T. M. Versatile Porous Poly(arylene ether)s via Pd-Catalyzed C−O Polycondensation. *J. Am. Chem. Soc.* **2021**, *143* (30), 11828−11835.
(20) Aitken, C. L.; Koros, W. J.; Paul, D. R. Effect of Structural Symmetry on Gas Transport Properties of Polysulfones. *Macromolecules* **1992**, *25* (13), 3424−3434.
(21) Robeson, L. M.; Burgoyne, W. F.; Langsam, M.; Savoca, A. C.; Tien, C. F. High Performance Polymers for Membrane Separation. *Polymer* **1994**, *35* (23), 4970−4978.
(22) Stern, S. A.; Mi, Y.; Yamamoto, H.; Clair, A. K. S. Structure/Permeability Relationships of Polyimide Membranes. Applications to the Separation of Gas Mixtures. *J. Polym. Sci., B: Polym. Phys.* **1989**, *27* (9), 1887−1909.
(23) Sykes, G. F.; St Clair, A. K. The Effect of Molecular Structure on the Gas Transmission Rates of Aromatic Polyimides. *J. Appl. Polym. Sci.* **1986**, *32* (2), 3725−3735.
(24) Tanaka, K.; Kusuki, Y.; Kita, H.; Okamoto, K.; Nakamura, A. Gas Permeability and Permselectivity in Homo- and Copolyimides from 3,3′,4,4′-Biphenyltetracarboxylic Dianhydride and 3,3′- and 4,4′-Diaminodiphenylsulfones. *Polym. J.* **1990**, *22* (5), 381−385.
(25) Wu, A. X.; Drayton, J. A.; Rodriguez, K. M.; Qian, Q.; Lin, S.; Smith, Z. P. Influence of Aliphatic and Aromatic Fluorine Groups on Gas Permeability and Morphology of Fluorinated Polyimide Films. *Macromolecules* **2020**, *53* (13), 5085−5095.
(26) Wu, A. X.; Drayton, J. A.; Rodriguez, K. M.; Benedetti, F. M.; Qian, Q.; Lin, S.; Smith, Z. P. Elucidating the Role of Fluorine Content on Gas Sorption Properties of Fluorinated Polyimides. *Macromolecules* **2021**, *54* (1), 22−34.
(27) Alghunaimi, F.; Ghanem, B.; Alaslai, N.; Swaidan, R.; Litwiller, E.; Pinnau, I. Gas Permeation and Physical Aging Properties of Iptycene Diamine-Based Microporous Polyimides. *J. Membr. Sci.* **2015**, *490*, 321−327.
(28) Cho, Y. J.; Park, H. B. High Performance Polyimide with High Internal Free Volume Elements. *Macromol. Rapid Commun.* **2011**, *32* (7), 579−586.
(29) Khan, N.; Itaya, K.; Wirth, T. Chiral Iodotriptycenes: Synthesis and Catalytic Applications. *ChemistryOpen* **2022**, *11* (7), No. e202200145.
(30) Clark, G. L.; Pickett, L. W. Crystal Structures of Some Derivatives of Diphenyl. *Proc. Natl. Acad. Sci. U.S.A.* **1930**, *16* (1), 20−27.
(31) Martinez, C. R.; Iverson, B. L. Rethinking the Term "Pi-Stacking. *Chem. Sci.* **2012**, *3* (7), 2191−2201.
(32) Hargreaves, A.; Rizvi, S. H. The Crystal and Molecular Structure of Biphenyl. *Acta Crystallogr.* **1962**, *15* (4), 365−373.
(33) Trotter, J. The Crystal and Molecular Structure of Biphenyl. *Acta Crystallogr.* **1961**, *14* (11), 1135−1140.
(34) Grein, F. Twist Angles and Rotational Energy Barriers of Biphenyl and Substituted Biphenyls. *J. Phys. Chem. A* **2002**, *106* (15), 3823−3827.
(35) Hernández-Trujillo, J.; Matta, C. F. Hydrogen-Hydrogen Bonding in Biphenyl Revisited. *Struct. Chem.* **2007**, *18* (6), 849−857.
(36) Wu, A. X.; Lin, S.; Mizrahi Rodriguez, K.; Benedetti, F. M.; Joo, T.; Grosz, A. F.; Storme, K. R.; Roy, N.; Syar, D.; Smith, Z. P. Revisiting Group Contribution Theory for Estimating Fractional Free Volume of Microporous Polymer Membranes. *J. Membr. Sci.* **2021**, *636*, No. 119526.
(37) Zhang, Z.; Ren, X.; Huo, G.; Kang, S.; Wang, Z.; Li, N. Tuning Interchain Cavity of Fluorinated Polyimide by DABA for Improved Gas Separation Performance. *J. Membr. Sci.* **2023**, *675*, No. 121485.
(38) Kim, Y. H.; Kim, H. S.; Kwon, S. K. Synthesis and Characterization of Highly Soluble and Oxygen Permeable New Polyimides Based on Twisted Biphenyl Dianhydride and Spirobifluorene Diamine. *Macromolecules* **2005**, *38* (19), 7950−7956.
(39) Chen, W.; Wu, K.; Qu, Z.; Lu, M. Intrinsic High Thermal Conductive Co-Polyester Based on Offset $\pi-\pi$ Stacking. *Eur. Polym. J.* **2019**, *121*, No. 109275.
(40) Corrado, T.; Guo, R. Macromolecular Design Strategies toward Tailoring Free Volume in Glassy Polymers for High Performance Gas Separation Membranes. *Mol. Syst. Des. Eng.* **2020**, *5* (1), 22−48.
(41) Wiegand, J. R.; Smith, Z. P.; Liu, Q.; Patterson, C. T.; Freeman, B. D.; Guo, R. Synthesis and Characterization of Triptycene-Based Polyimides with Tunable High Fractional Free Volume for Gas Separation Membranes. *J. Mater. Chem. A* **2014**, *2* (33), 13309−13320.
(42) Matteucci, S.; Yampolskii, Y.; Freeman, B. D.; Pinnau, I. Transport of Gases and Vapors in Glassy and Rubbery Polymers. In *Materials Science of Membranes for Gas and Vapor Separation*; John Wiley & Sons Ltd, 2006; pp 1−47.
(43) Thran, A.; Kroll, C.; Faupel, F. Correlation between Fractional Free Volume and Diffusivity of Gas Molecules in Glassy Polymers. *J. Polym. Sci., Part B: Polym. Phys.* **1999**, *37* (23), 3344−3358.
(44) Cohen, M. H.; Turnbull, D. Molecular Transport in Liquids and Glasses. *J. Chem. Phys.* **1959**, *31* (5), 1164−1169.
(45) Lin, H.; Freeman, B. D. Gas Permeation and Diffusion in Cross-Linked Poly(Ethylene Glycol Diacrylate). *Macromolecules* **2006**, *39* (10), 3568−3580.
(46) Wu, A. X.; Drayton, J. A.; Smith, Z. P. The Perfluoropolymer Upper Bound. *AIChE J.* **2019**, *65* (12), 1−12.
(47) Yampolskii, Y.; Belov, N.; Alentiev, A. Perfluorinated Polymers as Materials of Membranes for Gas and Vapor Separation. *J. Membr. Sci.* **2020**, *598*, No. 117779.
(48) Paul, D. R.; Yampolskii, Y. P. *Polymeric Gas Separation Membranes*; CRC Press: Boca Raton, FL, 1994.
(49) Smith, Z. P.; Tiwari, R. R.; Dose, M. E.; Gleason, K. L.; Murphy, T. M.; Sanders, D. F.; Gunawan, G.; Robeson, L. M.; Paul, D. R.; Freeman, B. D. Influence of Diffusivity and Sorption on Helium and Hydrogen Separations in Hydrocarbon, Silicon, and Fluorocarbon-Based Polymers. *Macromolecules* **2014**, *47* (9), 3170−3184.
(50) Paul, D. R.; Koros, W. J. Effect of Partially Immobilizing Sorption on Permeability and the Diffusion Time Lag. *J. Polym. Sci. A Polym. Phys.* **1976**, *14* (4), 675−685.
(51) Mizrahi Rodriguez, K.; Benedetti, F. M.; Roy, N.; Wu, A. X.; Smith, Z. P. Sorption-Enhanced Mixed-Gas Transport in Amine Functionalized Polymers of Intrinsic Microporosity (PIMs). *J. Mater. Chem. A* **2021**, *9* (41), 23631−23642.
(52) Wind, J. D.; Paul, D. R.; Koros, W. J. Natural Gas Permeation in Polyimide Membranes. *J. Membr. Sci.* **2004**, *228* (2), 227−236.
(53) Mizrahi Rodriguez, K.; Lin, S.; Wu, A. X.; Storme, K. R.; Joo, T.; Grosz, A. F.; Roy, N.; Syar, D.; Benedetti, F. M.; Smith, Z. P. Penetrant-Induced Plasticization in Microporous Polymer Membranes. *Chem. Soc. Rev.* **2024**, *53*, 2435−2529.
(54) Wind, J. D.; Paul, D. R.; Koros, W. J. Natural Gas Permeation in Polyimide Membranes. *J. Membr. Sci.* **2004**, *228* (2), 227−236.
(55) Mizrahi Rodriguez, K.; Lin, S.; Wu, A. X.; Storme, K. R.; Joo, T.; Grosz, A. F.; Roy, N.; Syar, D.; Benedetti, F. M.; Smith, Z. P. Penetrant-Induced Plasticization in Microporous Polymer Membranes. *Chem. Soc. Rev.* **2024**, *53*, 2435−2529.

https://doi.org/10.1021/acs.macromol.4c01199
Macromolecules 2024, 57, 7065−7073